Chapter 2
Theoretical Considerations for Laser Spectroscopy

2.1 Hyperfine Structure

The coupling of the electronic angular momentum with the nuclear angular momentum leads to a substructure of the energy levels of the electronic orbitals, known as the hyperfine structure. For the case of ^{221}Fr, the hyperfine structure arising from the coupling of its nuclear spin $I = 5/2^-$ with the electronic orbitals $7p\,^2S_{1/2}$ and $8p\,^2P_{3/2}$ is shown in Fig. 2.1.

The electron has two components of angular momentum: the spin angular momentum, S, and the orbital angular momentum, L. In light atoms (usually $Z < 30$), these couple (known as LS coupling) to give the total electronic angular momentum J,

$$J = L + S, \tag{2.1}$$

where

$$L = \sum_i l_i \text{ and } S = \sum_i s_i. \tag{2.2}$$

In heavier atoms such a lead, bismuth and polonium, the individual orbital angular momentum, l_i, and spin angular momentum, s_i, combine to form a individual total angular momentum, j_i. These couple to form the total orbital angular momentum, J. This is known as jj coupling,

$$J = \sum_i j_i = \sum_i (l_i + s_i). \tag{2.3}$$

The coupling of the different projections of the spin and orbital angular momenta gives rise to the fine structure of the electronic orbitals. The total electronic angular momentum, J, in turn couples to the nuclear spin angular momentum, I, to give the total angular momentum, F,

$$F = I + J. \tag{2.4}$$

K.M. Lynch, *Laser Assisted Nuclear Decay Spectroscopy*,
Springer Theses, DOI: 10.1007/978-3-319-07112-1_2

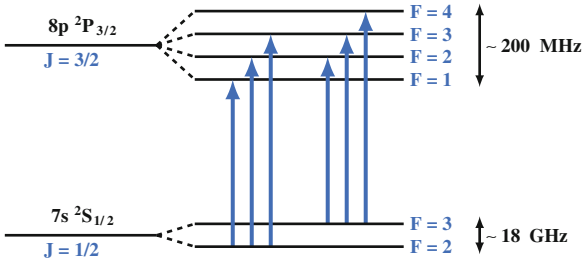

Fig. 2.1 Schematic illustration of the hyperfine structure of ^{221}Fr, where I = 5/2$^-$

When both I and J are greater then zero, degenerate hyperfine substates of the electronic orbitals are produced. The presence of the nuclear magnetic dipole moment or electric quadrupole moment raises the degeneracy of these substates, giving rise to a different energy for each level.

The perturbation of the hyperfine energy levels is given by [1, 2]

$$\frac{\Delta E}{h} = \frac{K}{2}A + \frac{3K(K+1) - 4I(I+1)J(J+1)}{8I(2I-1)J(2J-1)}B, \tag{2.5}$$

where $K = F(F+1) - I(I+1) - J(J+1)$. The hyperfine factors A and B are defined as

$$A = \frac{\mu_I B_e}{IJ}, \tag{2.6}$$

and

$$B = eQ_s\left\langle\frac{\partial^2 V_e}{\partial z^2}\right\rangle, \tag{2.7}$$

with μ_I the magnetic dipole moment of the nucleus, B_e the magnetic field of the electrons at the nucleus, Q_s the electric quadrupole moment, and $\langle\partial^2 V_e/\partial z^2\rangle$ the electric field gradient produced by the electrons.

The frequency, γ, at which the atomic transition between an upper and lower J level (J_u and J_l respectively) occurs is given by

$$\gamma = \nu + \alpha_{upper}A_{upper} + \beta_{upper}B_{upper} - \alpha_{lower}A_{lower} - \beta_{lower}B_{lower}. \tag{2.8}$$

Here, α and β are functions of the nuclear and atomic spin, as defined by

$$\alpha = \frac{K}{2}, \tag{2.9}$$

and

$$\beta = \frac{3K(K+1) - 4I(I+1)J(J+1)}{8I(2I-1)J(2J-1)}. \tag{2.10}$$

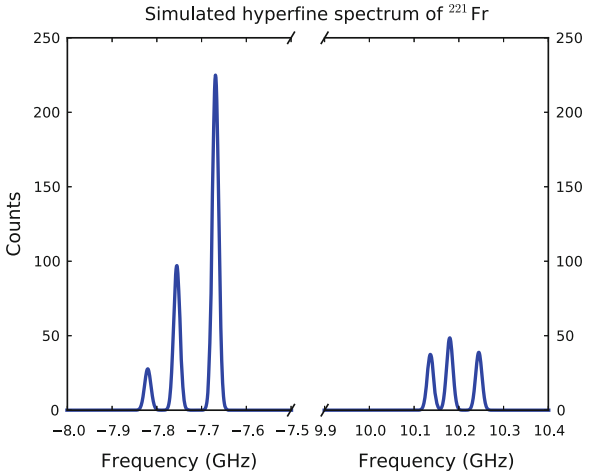

Fig. 2.2 Simulated hyperfine structure scan of ^{221}Fr. The lower $7p\,^2S_{1/2}$ state splitting is ∼18 GHz whereas the upper state splitting of $8p\,^2P_{3/2}$ is significantly smaller at ∼200 MHz

By fitting the hyperfine structure spectrum (such as one akin to Fig. 2.2) with a numerical routine such as χ^2-minimisation, the centroid frequency, ν, and the hyperfine factors $A_{upper,lower}$ and $B_{upper,lower}$ can be evaluated.

2.1.1 Nuclear Spin

For well resolved hyperfine structures, the nuclear spin of the isotope under investigation can often be determined from the relative frequencies of the atomic transitions, according to Eq. 2.5 if $J_{upper,lower} \leq 1/2$. In some cases, a spin can be immediately discounted due to the number of peaks present in the spectrum. For J = 1/2 to 1/2 or 0 to 1 transitions, the hyperfine structure does not provide enough information to determine the spin. For all other possible spins, χ^2 can be minimized and compared. The relative hyperfine-peak intensities determined by the weak-field angular coupling distribution can lead to a more significant difference in χ^2-minimisation [3]. However, careful experimental monitoring is required [4, 5].

2.1.2 Magnetic Dipole Moment

The magnetic dipole moment of the nucleus, μ_I, arises when the nuclear spin, I, is greater than zero. However, the magnitude of the magnetic moment when $I > 0$ can be vanishingly small, resulting in an A factor that leads to a hyperfine structure

that is smaller than the natural line width of the state [6]. As shown in Eq. 2.6, the magnetic moment of the nucleus can be extracted from the hyperfine A factor. To the first order, the magnetic field at the nucleus due to the electrons is uniform along an isotopic chain, in the same way the electronic angular momentum, J, is. For a discussion on higher order corrections, see Sect. 2.1.4. This allows the magnetic moment of the isotope under investigation to be extracted from the known moment of another isotope of the element, using the ratio

$$\mu = \mu_{ref} \frac{I A}{I_{ref} A_{ref}}. \tag{2.11}$$

2.1.3 Electric Quadrupole Moment

The electric quadrupole moment, Q_s, can be determined in a similar fashion, for nuclei with $I > 1/2$ and $J > 1/2$. This is a result of the electric field gradient $\langle \partial^2 V_e / \partial z^2 \rangle$ produced by the electrons remaining constant along an isotopic chain. The quadrupole moment can be extracted from the magnetic moment and hyperfine B factor of a reference isotope, using the ratio

$$Q_s = Q_{s,ref} \frac{B}{B_{ref}}. \tag{2.12}$$

2.1.4 Hyperfine Anomaly

The Bohr-Weisskopf effect (BW) corrects the assumption that the nuclear magnetization is point-like [7]. For the $S_{1/2}$ and $P_{1/2}$ atomic states, the hyperfine interaction is affected by the non-uniformity of the magnetic field over the nuclear volume. For all other states, this effect is zero since there is virtually no overlap with the nucleus [8]. For heavy nuclei, the BW-effect is small, of the order of 1 % of the hyperfine A factor [9].

In addition, the Breit-Rosenthal effect (BR) corrects for the charge volume of the nucleus [10]. This effect is small for light nuclei but much larger for heavier nuclei, of the order of 20 % for Z = 90 [9]. These two corrections reduce the hyperfine A factor to

$$A = A_{point-like}(1 - \epsilon_{BW})(1 + \epsilon_{BR}). \tag{2.13}$$

This leads to a modified expression for the magnetic moment,

$$\mu = \mu_{ref} \frac{I A}{I_{ref} A_{ref}} (1 + \Delta), \tag{2.14}$$

with,

$$\Delta = \frac{A\, g_{ref}}{A_{ref}\, g} - 1 \approx \epsilon - \epsilon_{ref}, \tag{2.15}$$

and the magnetic hyperfine anomaly defined as ϵ [11]. This can be calculated for nuclei whose nuclear gyromagnetic (g-) factors have been measured independent of laser spectroscopy, for example with nuclear magnetic resonance (NMR) spectroscopy [12].

The hyperfine anomaly can range from 10^{-5} to 1 % depending on the location of the isotope in the nuclear chart. For the francium isotopes, it is generally considered to be of the order of 1 % and is included as a contribution to the error [13].

2.2 Isotope Shift

The centre of gravity of the hyperfine structure (the centroid frequency) of one isotope relative to another, is shifted due to the difference in the structure of the two nuclei: their volume, shape, mass and charge radii. The isotopes shift, the shift of transition frequency of isotope A' compared to isotope A, can be written as

$$\delta\nu_{IS}^{A,A'} = \nu^{A'} - \nu^{A}. \tag{2.16}$$

The isotope shift can be evaluated as a linear combination of the mass shift and the field shift [14]

$$\delta\nu_{IS}^{A,A'} = \delta\nu_{MS}^{A,A'} + \delta\nu_{FS}^{A,A'}. \tag{2.17}$$

It arises (in part) due to the change in the mean-square charge radii between isotopes, associated with volume and shape changes.

2.2.1 Mass Shift

The mass shift component of the isotope shift originates from the recoil kinetic energy of a nucleus that has a finite mass. This shift can be calculated by

$$\delta\nu_{MS}^{A,A'} = M\frac{A' - A}{AA'}. \tag{2.18}$$

The M term, the mass factor, is dependent of the measured transition. For light nuclei, the mass shift is the significant contributing component of the isotope shift due to the $1/A^2$ dependence: the addition of a single neutron to a light nucleus has a much larger effect than adding one neutron to a heavy nucleus. The mass shift of an isomeric state relative to its ground state is zero as these nuclei have the same nuclear

composition but are in a different nuclear state. However, with respect to the overall trend, the mass shift for isomers needs to be included. The remaining field shift is renamed the isomer shift, and gives the difference in centroid frequency between the ground state and the isomeric state.

The mass factor can be approximated in terms of a linear combination of the normal mass shift, K_{NMS}, and the specific mass shift, K_{SMS},

$$M = K_{NMS} + K_{SMS}. \tag{2.19}$$

The normal mass shift (NMS) is the contribution expected for a two-body system: the correction to the energy levels of the electrons relative to an infinitely heavy nucleus. This is always positive for the heavier isotope [15]. The normal mass shift is transition frequency, ν_{expt}, dependent and can be expressed as

$$K_{NMS} = \frac{\nu_{expt}}{1{,}822.888}. \tag{2.20}$$

The specific mass shift (SMS) is caused by the correlations between the electrons and can cause both a positive or negative shift. Calculation of this shift is non-trivial due to the evaluation of electron-correlation integrals. *Ab initio* calculations are only possible for nuclei with up to three electrons [16]. Heavier systems rely on large-scale many-body calculations, which are less accurate [17]. Alternatively, if experimental data is available, the specific mass shift can be determined by use of a King plot analysis [18]. This method is outlined in Sect. 2.2.4.

2.2.2 Field Shift

In heavy atoms, the isotope shift is dominated by the field shift: the shift in energy caused by the change in nuclear charge distribution as the nuclear content changes. This modifies the Coulomb interaction with the electrons. Over the nuclear volume, constant electron density is assumed and the perturbation in the electronic energy levels can be shown (to a first order approximation) to equal the mean-square charge radius, given by

$$\langle r^2 \rangle = \frac{\int_0^\infty \rho(r) r^2 \mathrm{d}V}{\int_0^\infty \rho(r) \mathrm{d}V}, \tag{2.21}$$

where $\rho(r)$ is the nuclear density. The field shift is sensitive to the change in the mean-square charge radius, as shown by relativistic calculations [19], thus the field shift is given by

$$\delta\nu_{FS}^{A,A'} = \frac{\pi a_0^3}{Z} \Delta|\psi(0)|^2 f(Z) \delta\langle r^2 \rangle^{A,A'}, \tag{2.22}$$

where $\Delta|\psi(0)|^2$ is the change in the probability density function of the electrons at the nucleus, a_0 is the Bohr radius, and $f(Z)$ a relativistic correction factor [20]. For isotopes of the same element, the atomic transition between s and p electrons yield the largest field shifts and are thus more sensitive to the difference in the mean-square charge radius, $\delta\langle r^2\rangle^{A,A'}$.

2.2.3 Total Isotope Shift

The isotope shift [21] can therefore be expressed as

$$\delta\nu^{A,A'} = M\frac{A'-A}{AA'} + F\delta\langle r^2\rangle^{A,A'}. \tag{2.23}$$

This separates the atomic and nuclear dependences: M and F are purely dependent on the atomic transitions and by comparison, $(A'-A)/AA'$ and $\delta\langle r^2\rangle^{A,A'}$ contain only the nuclear properties information.

2.2.4 King Plot Analysis

The atomic factors F and M can be evaluated by way of a King plot [18] if data is available for more than two stable isotopes whose charge radii were determined by other techniques (muonic x-rays or electron scattering). When no experimental data is available, the extraction of the atomic factors relies upon theoretical calculations, and introduces atomic-model dependence. The King plot analysis compares the isotope shifts of an element from two different atomic transitions. Equation 2.23 is first multiplied by the modification factor,

$$\mu_{A,A'} = \frac{AA'}{A'-A}, \tag{2.24}$$

for the transitions i and j, giving,

$$\begin{aligned}\mu_{A,A'}\delta\nu_i^{A,A'} &= M_i + \mu_{A,A'}F_i\delta\langle r^2\rangle^{A,A'},\\ \mu_{A,A'}\delta\nu_j^{A,A'} &= M_j + \mu_{A,A'}F_j\delta\langle r^2\rangle^{A,A'}.\end{aligned} \tag{2.25}$$

After the elimination of $\mu^{A,A'}\delta\langle r^2\rangle$, the linear fit of the data $\mu^{A,A'}\delta\nu_j^{A,A'}$ against $\mu^{A,A'}\delta\nu_i^{A,A'}$ gives the straight line equation

$$\mu^{A,A'}\delta\nu_j^{A,A'} = \frac{F_j}{F_i}\mu^{A,A'}\delta\nu_i^{A,A'} + M_j - \frac{F_j}{F_i}M_i. \tag{2.26}$$

This has a gradient of F_j/F_i and an intercept of $M_j - (F_j/F_i)M_i$, whereby F and M can be evaluated for the transition of interest.

References

1. Schwartz C (1955) Phys Rev 97:380
2. Casimir HBG (1963) On the interaction between atomic nuclei and electrons. Freeman, San Francisco
3. Sato M (1955) Prog Theor Phys 13:405
4. Cheal B et al (2010) Phys Rev Lett 104:252502
5. Köster U et al (2011) Phys Rev C 84:034320
6. Mané E, Cheal B et al (2011) Phys Rev C 84:024303
7. Bohr A, Weisskopf VF (1950) Phys Rev 77:94
8. Grossman JS et al (1999) Phys Rev Lett 83:935
9. Büttgenbach S (1984) Hyperfine Interact 20:1
10. Rosenthal JE, Breit G (1932) Phys Rev 41:459
11. Barzakh AE et al (2012) Phys Rev C 86:014311
12. Panissod P (1986) Nuclear magnetic resonance, topics in current physics: microscopics models in physics. Springer, Berlin
13. Stroke HH et al (1961) Phys Rev 123:1326
14. King WH (1984) Isotope shifts in atomic spectra. Plenum, New York
15. Blaum K et al (2013) Phys Scripta 2013:014017
16. Yan ZC et al (2008) Phys Rev Lett 100:243002
17. Cheal B et al (2012) Phys Rev A 86:042501
18. King WH (1963) J Opt Soc Am 53:638
19. Bodmer AR (1953) Proc Phys Soc A 66:1041
20. Blundell SA et al (1985) Z Phys A 321:31
21. Cheal B, Flanagan KT (2010) J Phys G 37:113101

http://www.springer.com/978-3-319-07111-4

Laser Assisted Nuclear Decay Spectroscopy
A New Method for Studying Neutron-Deficient Francium Isotopes
Lynch, K.M.
2015, XIII, 131 p. 95 illus., 46 illus. in color., Hardcover
ISBN: 978-3-319-07111-4